Spectroscopy and autodetachment dynamics of PtN^-

Kermit K. Murray, Keith R. Lykke, and W. C. Lineberger
Joint Institute for Laboratory Astrophysics, University of Colorado and National Bureau of Standards, and Department of Chemistry and Biochemistry, University of Colorado, Boulder, Colorado 80309-0440
(Received 15 January 1987)

The negative ion PtN^- has been studied by autodetachment spectroscopy in a coaxial laser-ion beam spectrometer. Sharp resonances were observed at photon energies near the photodetachment threshold, and the sharp structure could be assigned as $^1\Pi(v=1)\leftarrow{}^1\Sigma(v=0)$ transition, followed by autodetachment of the $^1\Pi$ state. A rotational assignment was accomplished and the observed linewidths as a function of rotational energy elucidate the dynamics of the autodetachment process. Saturation of this transition and the resulting optical pumping dips give a unique method of determining the absolute cross section of the transition.

I. INTRODUCTION

The field of molecular negative-ion spectroscopy has seen a remarkable growth recently. As recently as 1983 only the anions C_2^- and OH^- had been studied with rotational state resolution.[1–6] Since then, the spectra of three diatomic[7–10] and three polyatomic[11–13] negative ions have been obtained using high-resolution autodetachment spectroscopy. Additionally, velocity-modulated infrared absorption spectroscopy,[14] which has been applied to positive ions with great success, has recently been used to obtain the infrared vibration-rotation spectra of several negative ions,[15–18] and promises to be a useful technique in negative-ion spectroscopy.

Autodetachment spectroscopy in a fast ion beam is an extremely sensitive technique; experiments have been performed at ion densities of less than 1 ion/cm^3 per quantum state.[3,4] It is also a sub-Doppler technique with linewidths as low as 20 MHz having been observed.[7] Linewidths not limited by the residual Doppler spread in the ion beam give the autodetachment rates of the negative-ion excited states, revealing the quantum-level-dependent dynamics of the autodetachment process. Autodetachment spectroscopy is limited, however, by the lack of bound excited electronic states of negative ions. Molecules possessing dipole bound anion states are a class of negative ions accessible to electronic spectroscopy, but such states are limited to anions for which the dipole moment of the neutral core exceeds $\sim$2 D. Vibrational autodetachment spectroscopy is a more general, yet sensitive, technique, but photon absorption must result in electron ejection for this process to be observable.

A large class of negative ions that should be amenable to autodetachment spectroscopy is that of negative ions of transition-metal compounds.[7] The unoccupied d orbitals of many transition-metal atoms often lead to low-lying electronic states in transition-metal compounds. If a low-lying electronic state lies close in energy to the neutral-molecule electron affinity, autodetachment spectroscopy can often be carried out on the electronic transition from the ground state to this excited electronic state. Transition-metal systems must be chosen carefully, however, as the presence of many electronic and spin-orbit transitions in spectral regions of interest will lead to congested or highly perturbed spectra.[7]

We chose to study the PtN^- system in part because the isoelectronic PtO is known[19] to have a $^1\Sigma$ ground state which could lead to a simple electronic spectrum. Broad resonances in the photodestruction spectrum of PtN^- had also been observed[20] in a region easily accessed by a tunable single-mode cw dye laser. We present here a high-resolution study of an electronic transition in PtN^- with an autodetaching final state. The spectrum is assigned and the line assignments together with the observed linewidths give us insight into rotational and vibrational electronic energy transfer and the importance of autodetachment transition propensity rules. We also observe optical pumping dips[21] in the saturated electronic transition, a phenomenon providing a unique method for determining the absolute cross section for the bound-bound transition.

II. EXPERIMENTAL

The coaxial laser-ion beam spectrometer used in this study has been described in detail elsewhere,[11,22] and will only be briefly outlined here. The apparatus begins with an ion source from which negative ions are extracted, mass selected, and accelerated to 2 keV. The ion beam is merged with a cw laser beam by an electrostatic quadrupole deflector. The ion and laser beams interact over a 30-cm path before the ion beam is again bent by a second quadrupole deflector. Neutral species produced by photodetachment or photodissociation along the interaction path are unaffected by the second deflector and strike a CaF_2 plate. Secondary electrons ejected from the plate are detected by a ceramic electron multiplier. Low-energy ($<$200 meV) electrons produced by photodetachment are confined by a weak ($\sim$6 G) solenoidal magnetic field, and directed into a second electron multiplier.

The PtN^- ions were produced in a cold cathode sputter source of simple design.[20] A discharge is created in N_2 gas between a 35-mm diameter platinum cathode disk and a tantalum anode disk (spider plate) of roughly the same

diameter with holes symmetrically placed off center so as to shield the extraction aperture from free electrons in the plasma. Negative ions are extracted through a 2 mm hole 4 mm behind the anode disk into the low-pressure region of the apparatus. Typical sputtering conditions were 40 mTorr of N_2 gas with a discharge of 10 mA at 4 kV and a cathode-anode distance of 40 mm. Currents of typically 30 pA of PtN^- were obtained following mass selection, although periodic cleaning of sputtered platinum from the anode plate and glass walls of the source was necessary to obtain an optimum and stable ion beam.

The laser used in this experiment was a home-built cw dye laser using either R6G or DCM dyes pumped by all lines of an argon-ion laser. The laser could be scanned in three different configurations. For broadband scans the laser was configured as a standing-wave cavity with a birefringent tuner as the only tuning element. In this way, the entire dye range could be scanned with the tuner at a laser linewidth of ~ 0.5 cm^{-1}. The addition of a thin étalon to this configuration reduced the laser linewidth to ~ 0.05 cm^{-1}, but limited the tuning range to the ~ 6-cm^{-1} free spectral range of the thin étalon. For single-mode operation the laser was configured as a ring cavity and tuned with a rotating brewster plate. A thick étalon was locked to the cavity mode to prevent mode hopping during a scan. The laser could be tuned up to 1 cm^{-1} in this configuration. Additionally, the ring configured laser could be locked to an external reference cavity to reduce frequency drift below ~ 1 MHz/s. Although the residual Doppler spread of the ion beam is approximately 30 MHz, locking to the external cavity was found to reduce the noise level in single-mode scans of long duration. Output powers of up to 1.5-W broadband and 800-mW single mode were obtained using up to 10 W of pumping power from the argon-ion laser. The laser line shape was monitored by a Fabry-Perot interfermoter, absolute wavelength calibration with a precision of ± 0.003 cm^{-1} was performed using a traveling Michelson interferometer,[23] using a polarization stabilized He-Ne laser[24] as a reference. Line positions were corrected for a first-order Doppler shift of approximately 2 cm^{-1}.

III. RESULTS AND DISCUSSION

A. Spectroscopy and autodetachment dynamics

Figure 1(a) shows a broadband scan of PtN^- in the region from 14 500 to 17 300 cm^{-1}. It shows features identical to those observed in the previous study[20] in the 16 300 to 17 300-cm^{-1} region. Although this earlier work detected only neutral species and hence could not differentiate between photodetachment and photodissociation, we positively identify the features in Fig. 1(a) as being due to photodetachment, since all features appear in both the electron and neutral spectra. The features in the photodetachment spectrum arise from autodetaching PtN^- electronic states accessed from the ground or low-lying electronic states of PtN^-. It is not possible at this resolution to assign definitely the vibrational, spin-orbit, or electronic states involved in the transitions. Figure 1(b) shows the region of the PtN^- spectrum from 16 250 to 16 450 cm^{-1} scanned more slowly at the same laser linewidth. Sharper resonances are seen on the left shoulder of the peak, separated by ~ 2–3 cm^{-1} and apparently laser linewidth limited in width.

Figure 1(c) shows one of these sharp resonances in a

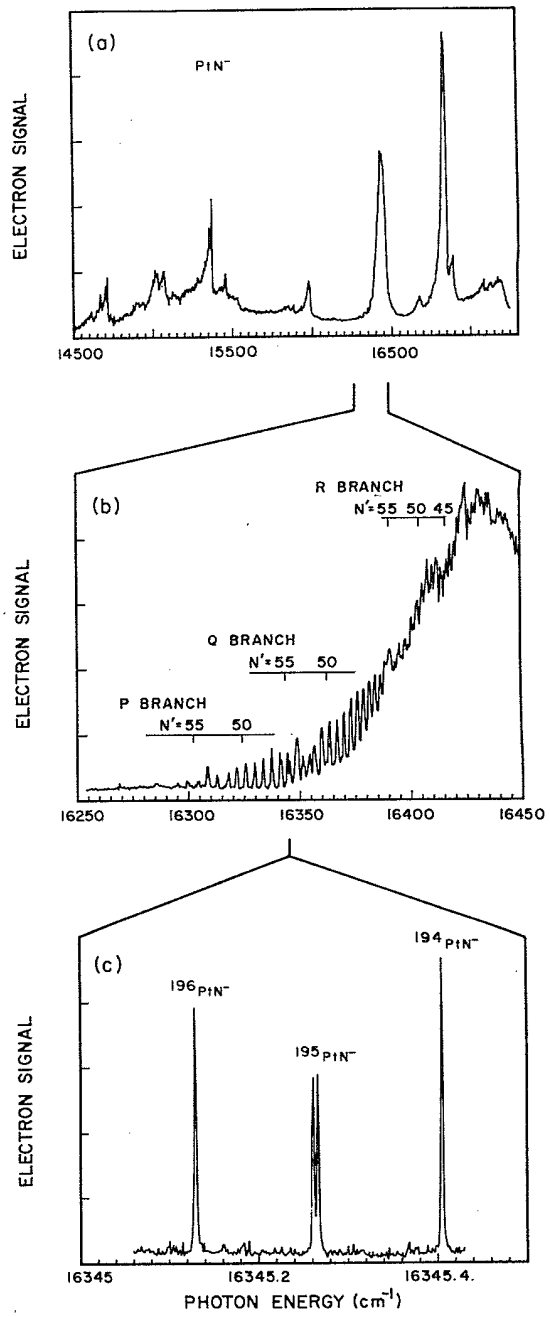

FIG. 1. (a) Broadband scan of PtN^-. The structure arises from autodetaching electronic states of PtN^-. (b) Broadband scan of PtN^- over the marked 200-cm^{-1} region of (a) showing sharp resonances. Upper-vibronic-state rotational quantum numbers are indicated for the regions of the *P*, *Q*, and *R* branches in which sharp resonances are observed. (c) Single-mode laser scan over the *a* single marked peak of (b). The $^{194}PtN^-$, $^{195}PtN^-$, and $^{196}PtN^-$ isotopes are clearly seen. Note the hyperfine splitting of $^{195}PtN^-$. The $^{198}PtN^-$ species is also observed at a different mass selector setting. See text for details.

10-GHz scan in the single-mode laser configuration. Each peak observed in the broadband scan is now resolved as three evenly spaced peaks of approximately equal intensity, with the central feature split into a doublet. If the mass selection magnet is tuned to slightly lower mass, it is found that for every set of three peaks, the highest energy peak gains intensity while the peak to lower photon energy loses intensity. The opposite intensity shift is seen when the mass selection magnet is tuned to slightly higher mass, and in addition a new weaker peak is observed at lower photon energy. The distance between this new peak and its nearest neighbor is approximately twice the spacing between neighboring peaks of the original three. This observation is consistent with isotope splitting in a platinum compound. The natural abundances of the ^{194}Pt, ^{195}Pt, ^{196}Pt, and ^{198}Pt isotopes are 32.9%, 33.8%, 25.3%, and 7.2%, respectively.[25] Thus we are observing the platinum isotope splitting with ^{194}PtN$^-$ transitions occurring at higher photon energies, and ^{196}PtN$^-$ transitions occurring at lower photon energies. The ^{198}PtN$^-$ transitions are weaker and only observed when the mass selection magnet is tuned to higher mass. The intensity of the ^{198}PtN$^-$ transition is consistent with the natural abundance of ^{198}Pt and provides further verification of the isotope assignment.

The entire spectral region from 14 500 to 17 300 cm^{-1} was scanned at a resolution adequate to observe narrow features, but narrow resonances were observed only in the region between 16 280 and 16 420 cm^{-1}. Broad resonances (>0.5 cm^{-1}) were observed in the regions between 15 470 and 15 490 cm^{-1} and between 16 720 and 16 780 cm^{-1}, but they could not be assigned. Forty transitions were observed between 16 280 and 16 420 cm^{-1} for each of ^{194}PtN$^-$, ^{195}PtN$^-$, and ^{196}PtN$^-$. These transitions were separated into three branches, easily identified by a broadening of the lines in each branch with increasing transition energy. Provisional N assignments and B values were obtained using the method of combination differences.[26] These assignments were confirmed in the least-squares fit described below. Fewer than 15 transitions were observed for each branch, with the *smallest* upper-state N value being 44. This small range of upper-state N values occurs because upper rotational states with $N \leq 44$ autodetach rapidly, leading to broad autodetachment resonances which are difficult to distinguish from the direct detachment background. Upper rotational states with $N \geq 59$ have long autodetachment lifetimes, so that ions optically excited to these states survive the ~ 10 μs interaction time without autodetaching and are again unobservable.

A nonlinear least-squares fit of all observed line positions was performed assuming that the ground state of

TABLE I. Spectroscopic constants for PtN$^-$. All values are in cm^{-1}. Numbers in parentheses are the 95% confidence error in the final digits. Note that although some of the constants are identical within experimental error, each column of numbers is the result of an independent calculation.

	^{194}PtN$^-$	^{195}PtN$^-$ [a]	^{196}PtN$^-$
B'	0.401(1)	0.401(1)	0.400(1)
D'	$1.6(2)\times10^{-6}$	$1.6(2)\times10^{-6}$	$1.6(2)\times10^{-6}$
B''	0.429(1)	0.428(1)	0.428(1)
D''	$0.4(2)\times10^{-6}$	$0.4(2)\times10^{-6}$	$0.4(2)\times10^{-6}$
T_v	16445.3(6)	16445.4(6)	16445.5(6)
q	$2.4(1)\times10^{-4}$	$2.4(1)\times10^{-4}$	$2.4(1)\times10^{-4}$
		$\Delta\nu_v = 0.351(4)$ [b]	

[a]Hyperfine splitting for ^{195}PtN$^-$ transitions was found to be 175(11) MHz for the Q branch and 85(5) MHz for the P and R branches, and was independent of rotational quantum numbers within experimental error.

[b]Vibrational isotope splitting between ^{196}PtN$^-$ and ^{194}PtN$^-$. See text for details.

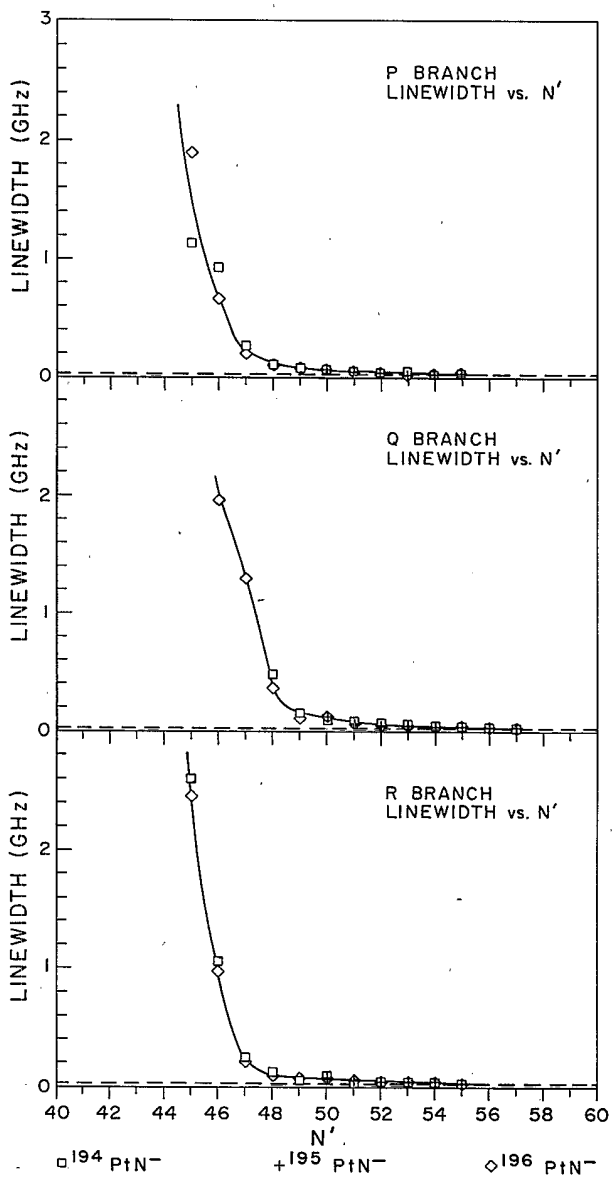

FIG. 2. Observed transition linewidths of the P, Q, and R branches plotted against the rotational quantum number of the upper (autodetaching) vibronic state. The residual Doppler spread of the ion beam is approximately 30 MHz, as indicated by the dashed lines.

PtN^- is $^1\Sigma$ as is the case for the isoelectronic neutral molecule PtO.[19] Since Q-branch transitions are observed, the upper state must have $\Lambda \neq 0$ and hence a Λ-doubling constant q was included in the upper-state energy expression. Distortion constants were also included for both the upper and lower states but higher-order corrections were ignored. The fit to all six constants was performed independently for each of $^{194}PtN^-$, $^{195}PtN^-$, and $^{196}PtN^-$ yielding the results listed in Table I. The magnitude of the Λ-doubling constant and the strength of the transition (see Sec. III B) indicates that the upper state is a Π state and, based on our assumption of a $^1\Sigma$ ground state, indicates that the transition is $^1\Pi \leftarrow {}^1\Sigma$.

A plot of the isotope splitting between the $^{194}PtN^-$ and the $^{196}PtN^-$ lines versus the average distance to the origin was fit to a straight line, the intercept of which gives the vibrational isotope splitting listed in Table I. The magnitude and sign of the isotope splitting indicates that the vibrational quantum number of the final state is one greater than the initial state. Since the transition energy is very nearly equal to the electron affinity of PtN,[27] we assert that the initial state is $v''=0$ and thus the final state $v'=1$.

The absorption profile of an autodetachment (or autoionization) line is known to have a Fano line shape.[28] However, when direct photodetachment has a much lower cross section than autodetachment, the resulting line shape is nearly symmetric and it is possible to fit the autodetachment resonances to a Lorentzian profile, rather than a Fano interference profile.[4] The above criterion is met in the case of PtN^- where direct detachment is at least 1000 times weaker than autodetachment. Thus the widths of the autodetachment resonances are related to the final-state lifetimes through the Heisenberg uncertainty principle. A plot of the observed linewidths for the P, Q, and R branch transitions against the rotational quantum number of the final state is shown in Fig. 2. The linewidths of the transitions with the same upper N value are the same within experimental error for the P and R branches but different from that obtained for the Q branch. For example, $N'=48$ transitions of the Q branch have linewidths of $\sim$410 MHz while $N'=48$ transitions of the P and R branches have linewidths of $\sim$110 MHz. This indicates that the upper N states have two Λ-doublet components with different autodetachment rates, one accessed in a Q transition, the other in a P or R transition. This is further indication of a $^1\Pi$ upper state.

Another result depicted in Fig. 2 is the *decrease* in linewidth and hence autodetachment rate with *increasing* N. This is the opposite of the results of all previous autodetachment studies, where increasing angular momentum was always found to coincide with decreased autodetachment lifetime.[7–9,11–13] To understand this phenomenon we must more closely examine the energetics and resulting angular momentum constraints for the system.

The T_v' value from Table I coupled with the PtN electron affinity[27] indicates that the $N=1$ level of PtN^- $^1\Pi$ ($v=1$) lies approximately 100 cm^{-1} above the $v=0$, $N=1$ level of PtN. Low N states of PtN^- $^1\Pi$ ($v=1$) may thus autodetach to PtN with no change in rotational angular momentum, a rapid process since there is no angular momentum barrier. This process gives rise to linewidths too large to distinguish from the direct detachment continuum. Since the rotational constant of PtN is larger[27] than the rotational constant of the PtN^- autodetaching state, this $\Delta N=0$ channel must close for some N, at which point the most favorable change in angular momentum will be $\Delta N=-1$. The $\Delta N-1$ channel will close for some higher N to be replaced by $\Delta N=-2$, etc. Each successively larger change in angular momentum will lead to a larger angular momentum barrier for the departing electron, and thus a lower autodetachment rate. Thus the autodetachment rate will *decrease* with *increasing* N of the autodetaching PtN^- state.

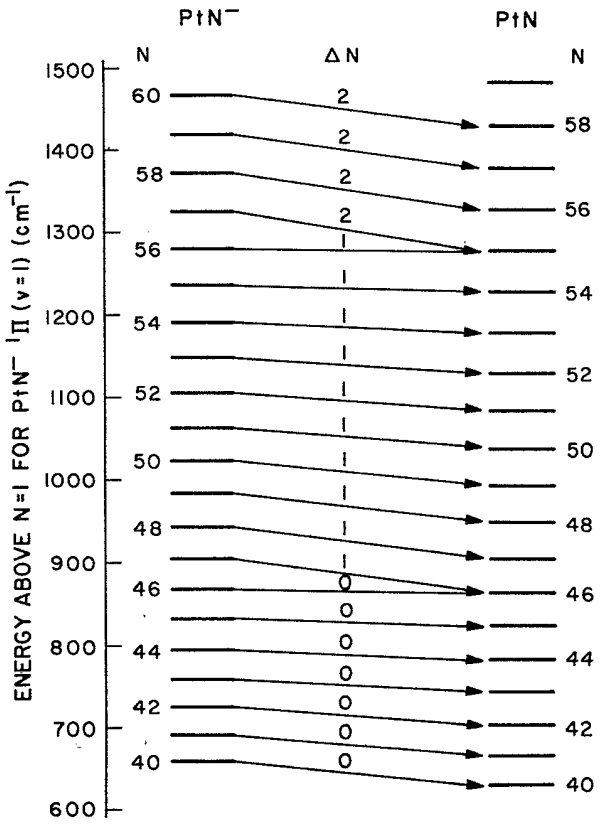

FIG. 3. Simplified energy-level diagram for PtN^- (left) and PtN (right) showing rotational levels and the most facile autodetachment transition for each level. The PtN^- Λ-doublet levels are not shown; at $N=50$ the levels are $\sim$0.6 cm^{-1} apart.

To quantify this result we note that the autodetachment lines begin to narrow at approximately $N'=45$. If we take the $N'=45$ level to be the energy at which the $\Delta N=0$ channel closes, then $N=45$ of the ground-state neutral must occur at the same energy. We have obtained the rotational constant of PtN using the anion ground-state rotational constant from Table I, coupled with the difference in bond length between the ground state of the anion and the ground state of the neutral indicated by a Franck-Condon analysis of the photoelectron spectrum of PtN^-.[27] Using the resulting rotational constant for PtN of 0.45 cm^{-1} and assuming the $N=45$ levels have the same energy, we independently obtain the electron affinity

of PtN consistent with the 16 350(80)-cm^{-1} photoelectron spectroscopic value.[27] This same calculation shows that the $\Delta N=-1$ channel will close at $N'=57$. This is remarkably close to the point where the PtN^- autodetaching state lifetimes increase to the point where they survive the approximately 10-μs transit of the spectrometer with no autodetachment and are not observed. An energy level diagram depicting the rotational energy levels of PtN^- $^1\Pi$ ($v=1$) and the ground electronic and vibrational state of PtN is given in Fig. 3.

B. Optical pumping dips

During the course of the experiment, we found that our dye-laser output power was sufficient to saturate the autodetachment transition. Additionally, for transitions with large autodetachment rates, we were able to deplete the ion ground-state population prior to ion entry into the region of efficient electron collection, creating optical pumping dips.[21] Figure 4 shows a typical optical pumping dip in the electron channel and simple saturation broadening in the neutral channel. Optical pumping dips occur in the electron channel because the ion beam interacts with the laser beam for a few (~ 3) centimeters before entering the electron collection solenoid. In this region PtN^- ions are optically pumped to an excited state, which subsequently autodetaches before the ion enters the electron collector. In this way the PtN^- ground-state population is depleted by photodetachment but no electron signal is observed. Since the optical pumping rate is faster on the center of the transition than it is when off center, the ground-state population entering the electron collector is smaller when the laser is tuned to the center of the transition, leading to a decrease in the observed signal at the peak center. There is no optical pumping dip in the neutral channel since all neutrals created along the interaction path are detected with approximately equal efficiency.

Optical pumping dips have been observed previously by Carrington and co-workers in the predissociation spectra of CH^+ (Ref. 29) and HeH^+.[30] Optical pumping dips provide a uniquely simple method for determining the absolute cross section of an autodetachment transition, as well as a way to observe subnatural linewidths.[21] If the fluorescence rate from the negative-ion excited state to the ground state is slow compared to autodetachment, and the autodetachment cross section is large enough (see below), an optical pumping dip will occur. The energy difference between the maxima produced by the dip (the "splitting") is given by[21]

$$\delta=2\gamma(\sigma\Phi\tau-1)^{1/2},$$

where 2γ is the natural width of the transition, σ is the transition cross section, Φ is the laser flux, and τ is the interaction time before electron collection becomes efficient. As can be seen from the equation, optical pumping dips occur only when $\sigma\Phi\tau>1$. For the transition shown in Fig. 4, $\delta\sim 100$ MHz, $2\gamma\sim 70$ MHz, $\Phi\sim 10^{19}$ photon/s cm^2, and $\tau\sim 1$ μs. These quantities yield an order of magnitude estimate of the absolute cross section of 10^{-13} cm^2.

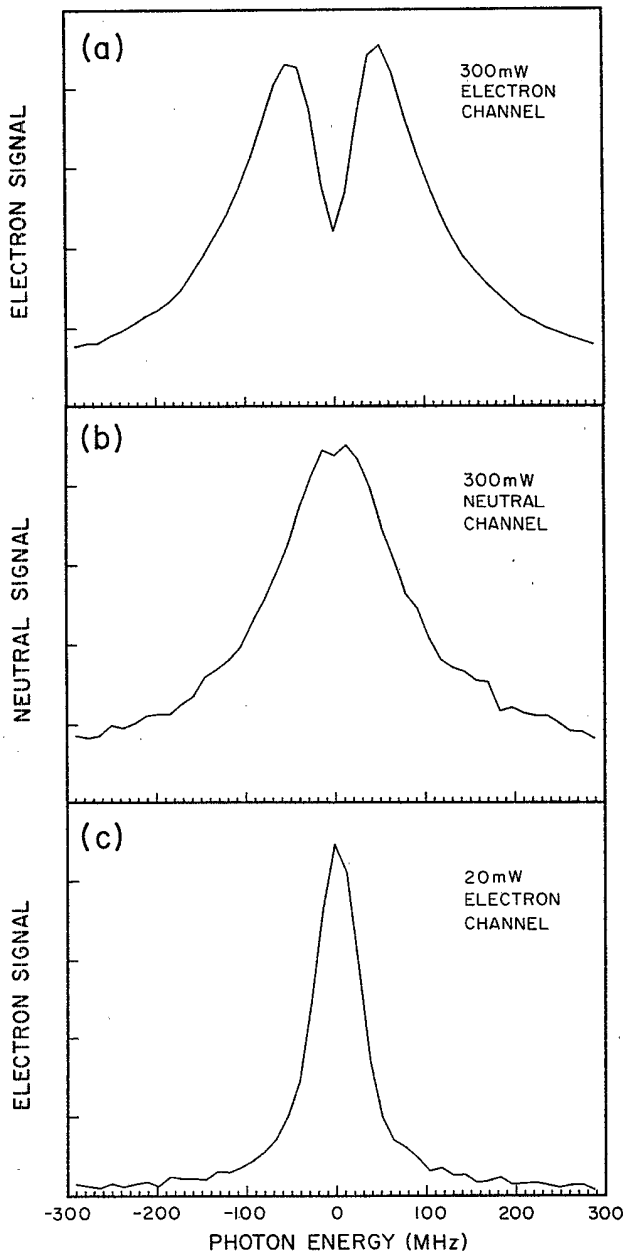

FIG. 4. Optical pumping dip of the $P(51)$ line of $^{196}PtN^-$. The dip occurs *only* in the electron channel due to ion-photon interaction prior to electron collection.

IV. CONCLUSION

We have investigated an electronic transition in PtN^- with an autodetaching final state which we assign as $^1\Pi$ ($v=1$)$\leftarrow{}^1\Sigma$ ($v=0$). The observed linewidths show that the autodetachment rate is strongly dependent on the angular momentum change between the anion and neutral upon electron detachment, with rates decreasing as the angular momentum barrier for the departing electron increases. The propensity for autodetachment with the smallest change in rotational angular momentum dom-

inates the autodetachment process. This phenomenon is underscored by the fact that rotational states with an open $\Delta N=0$ autodetachment channel autodetach more than 100 times more rapidly than states with 500 cm^{-1} greater rotational energy but with no facile route to autodetachment.

We have observed optical pumping dips which allow us to estimate the absolute cross section of the electronic transition. The relatively large value for the cross section ($\sim 10^{-13}$ cm^2) suggests that other transition-metal compounds and possibly transition metal clusters, if chosen carefully, are suitable systems for study using autodetachment spectroscopy.

ACKNOWLEDGMENTS

We wish to thank the National Science Foundation for support of this work under Grants No. CHE83-16628 and No. PHY86-04504. The nonlinear least-squares calculations included in this work were done on the JILA VAX 8600.

[1]G. Herzberg and A. Lagerqvist, Can. J. Phys. **46**, 2363 (1968).
[2]W. C. Lineberger and T. A. Patterson, Chem. Phys. Lett. **13**, 40 (1972).
[3]P. L. Jones, R. D. Mead, B. E. Kohler, S. D. Rosner, and W. C. Lineberger, J. Chem. Phys. **73**, 4419 (1980).
[4]U. Hefter, R. D. Mead, P. A. Schulz, and W. C. Lineberger, Phys. Rev. A **28**, 1429 (1983).
[5]R. D. Mead, U. Hefter, P. A. Schulz, and W. C. Lineberger, J. Chem. Phys. **82**, 1723 (1985).
[6]P. A. Schulz, R. D. Mead, P. L. Jones, and W. C. Lineberger, J. Chem. Phys. **77**, 1153 (1982).
[7]T. Andersen, K. R. Lykke, D. M. Neumark, and W. C. Lineberger, J. Chem. Phys. **86**, 1858 (1987).
[8]D. M. Neumark, K. R. Lykke, T. Andersen, and W. C. Lineberger, J. Chem. Phys. **83**, 4364 (1985).
[9]M. Al-za'al, H. C. Miller, and J. W. Farley, Chem. Phys. Lett. **131**, 56 (1986).
[10]R. C. Stoneman and D. J. Larson, J. Phys. B **19**, 405 (1986).
[11]K. R. Lykke, R. D. Mead, and W. C. Lineberger, Phys. Rev. Lett. **52**, 2221 (1984); R. D. Mead, K. R. Lykke, W. C. Lineberger, J. Marks, and J. I. Brauman, J. Chem. Phys. **81**, 4883 (1984).
[12]K. R. Lykke, D. M. Neumark, T. Andersen, V. J. Trapa, and W. C. Lineberger, in *Laser Spectroscopy* VII, edited by Y. R. Shen and T. W. Hänsch (Springer-Verlag, Berlin, 1985), p. 130.
[13]J. Marks, J. I. Brauman, R. D. Mead, K. R. Lykke, and W. C. Lineberger (unpublished).
[14]C. S. Gudeman and R. J. Saykally, Ann. Rev. Phys. Chem. **35**, 387 (1984).
[15]J. C. Owrutsky, N. H. Rosenbaum, L. M. Tack, and R. J. Saykally, J. Chem. Phys. **83**, 5338 (1985); N. H. Rosenbaum, J. C. Owrutsky, L. M. Tack, and R. J. Saykally *ibid.* **84**, 5308 (1986).
[16]K. Kawaguchi and E. Hirota, J. Chem. Phys. **84**, 2953 (1986).
[17]B. D. Rehfuss, M. W. Crofton, and T. Oka, J. Chem. Phys. **85**, 1785 (1986).
[18]L. M. Tack, N. H. Rosenbaum, J. C. Owrutsky, and R. J. Saykally, J. Chem. Phys. **84**, 7056 (1986).
[19]R. Scallman, U. Sassenberg, and C. Nilsson, Can. J. Phys. **53**, 1991 (1975), and references therein.
[20]H. Hotop and W. C. Lineberger, J. Chem. Phys. **58**, 2379 (1973).
[21]C. M. Klimcak and J. C. Camparo, Phys. Rev. A **30**, 1791 (1984).
[22]R. D. Mead, Ph. D. thesis, University of Colarado, 1984.
[23]J. L. Hall and S. A. Lee, Appl. Phys. Lett. **25**, 367 (1976).
[24]R. Balhorn, H. Kunzmann, and F. Lebowsky, Appl. Opt. **11**, 742 (1972).
[25]R. C. Weast, *Handbook of Chemistry and Physics*, 66th ed, (Chemical Rubber, Orlando, 1985).
[26]G. Herzberg, *Spectra of Diatomic Molecules* (Van Nostrand, Princeton, 1950).
[27]D. G. Leopold, K. Ervin, J. Ho, and W. C. Lineberger (unpublished).
[28]U. Fano, Phys. Rev. **124**, 1866 (1961).
[29]A. Carrington, J. Buttenshaw, R. A. Kennedy, and T. P. Softley, Mol. Phys. **45**, 747 (1982).
[30]A. Carrington, R. A. Kennedy, T. P. Softley, P. G. Fournier, and E. G. Richard, Chem. Phys. **81**, 251 (1983).